




# Supplementary Information: Anisotropic Band Evolution of Bulk Black Phosphorus Induced by Uniaxial Tensile Strain

Yafeng Deng<sup>1\*</sup>, Yilin Zhang<sup>2</sup>, Yafei Zhao<sup>3</sup> , Yongkang Xu<sup>1</sup>, Xingze Dai<sup>1</sup>, Shuanghai Wang<sup>1</sup>, Xianyang Lu<sup>1</sup>, Yao Li<sup>1</sup>, Yongbing Xu<sup>1</sup> , and Liang He<sup>1</sup> 

<sup>1</sup> National Key Laboratory of Spin Chip and Technology, School of Electronic Science and Engineering, Nanjing University, Nanjing 210023, China.

<sup>2</sup> College of Optical and Electronic Technology, China Jiliang University, Hangzhou 310018, China.

<sup>3</sup> School of Physics and Engineering, Henan University of Science and Technology, Luoyang 471023, China.

## 1. The dispersion - $k$ relationships in Bulk BP

The dispersion- $k_x$  relationship along the **Z-L** direction exhibits a quasi-linear feature (red dashed line), while the dispersion- $k_y$  relationship along the **Z-A** direction follows a quadratic shape (red dashed line).

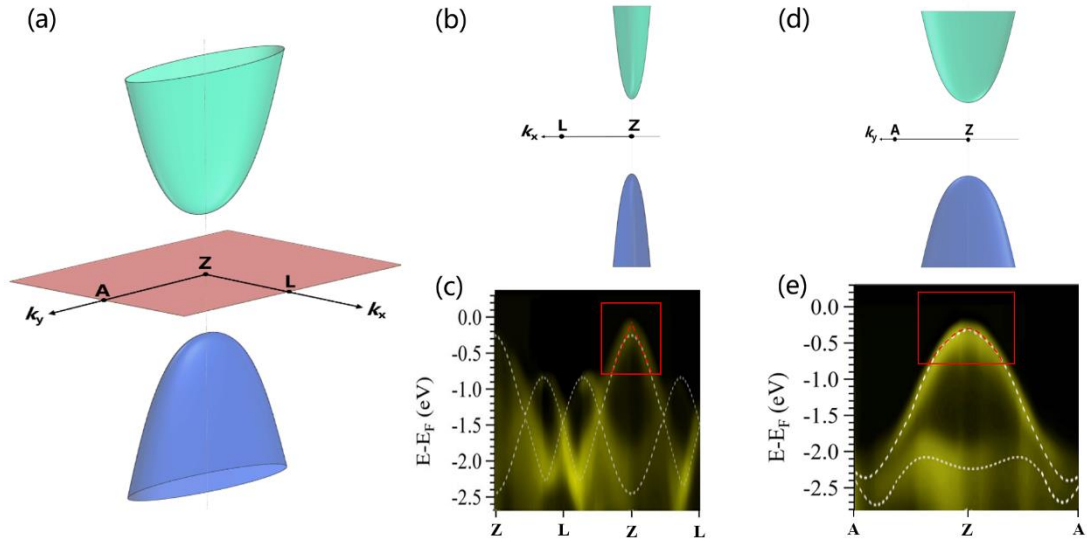


**Figure S1.** (a) The anisotropic band characteristics of bulk BP. (b, c) **Z-L** direction in BZ. (d, e) **Z-A** direction in BZ.

## 2. The Raman-shift curves of uniaxial tensile strain along various directions

As shown in Figure S2 (a-c), when applying tensile strain along the armchair direction of bulk BP, the  $A_g^1$  mode exhibits a slight redshift in Raman frequency, while the other two modes,  $B_{2g}$  and  $A_g^2$  display a significant blueshift in Raman frequency. This observation indicates the introduction of tensile strain in the armchair direction of the bulk BP lattice.

As shown in Figure S2 (d-f), When applying uniaxial tensile strain along the zigzag direction of the bulk BP, the phonon vibrations in the  $A_g^1$  mode,  $B_{2g}$  mode, and  $A_g^2$  mode all exhibit a characteristic redshift in Raman frequency. This observation confirms the introduction of effective tensile strain in the zigzag direction of the bulk BP lattice.

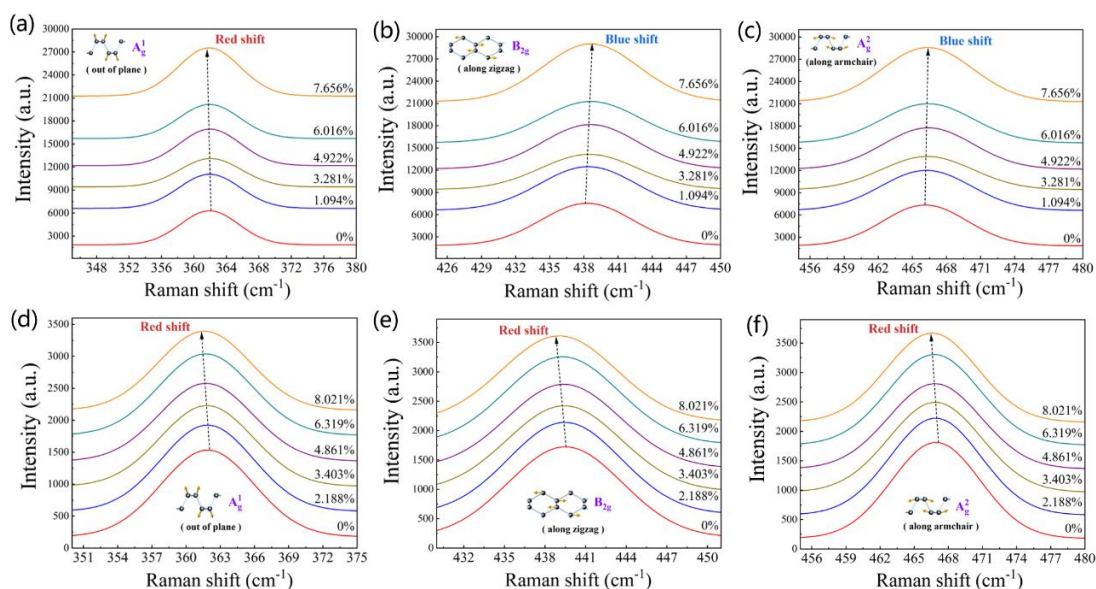


**Figure S2.** The Raman shifts of bulk BP regulated by uniaxial tensile strain along various directions (Corresponding to Figure 2b and 2d). The tensile strain along the armchair direction in figure (a-c), and the tensile strain along the zigzag direction in figure (d-f).

### 3. The calculated VBM shifts of bulk BP under uniaxial tensile strain

When the uniaxial tensile strain is applied along the armchair direction, the calculated VBM shifts exhibit a consistent monotonic trend with strain, towards deeper levels. From -211.3 meV to -306.3 meV, the maximum VBM shift of -95 meV closely approximated the experimental results (-100 meV).

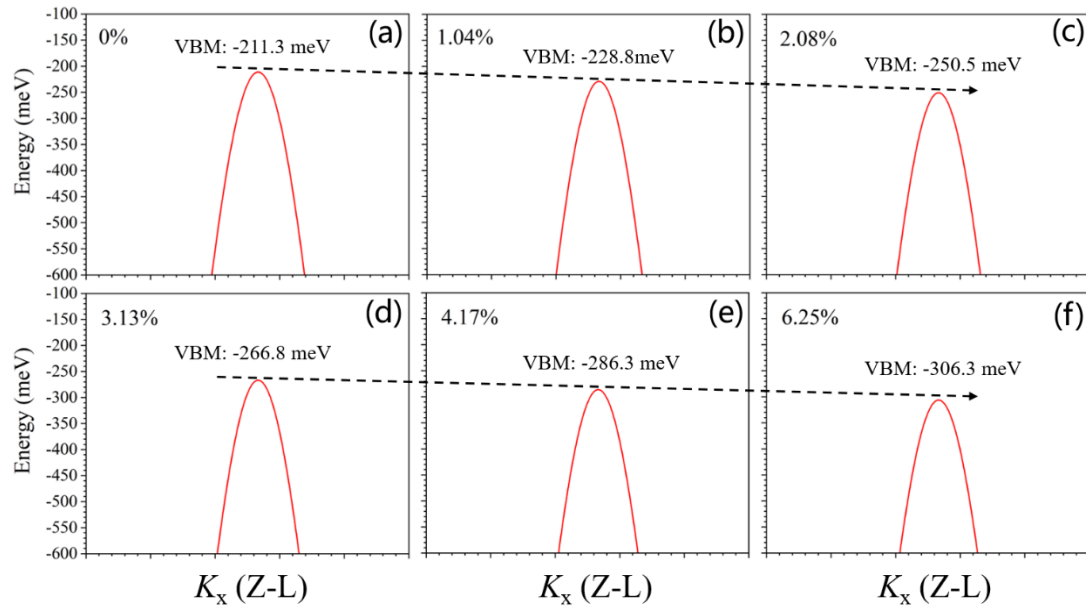


**Figure S3.** The calculated results when the tensile strain along armchair direction.  
(Corresponding to Figure 5a)

The VBM shifts induced by tensile strain along the zigzag direction exhibit VBM behavior entirely distinct from that along the armchair direction. The VBM shift of 104.3 meV is also basically the same as the experimental results (110 meV).

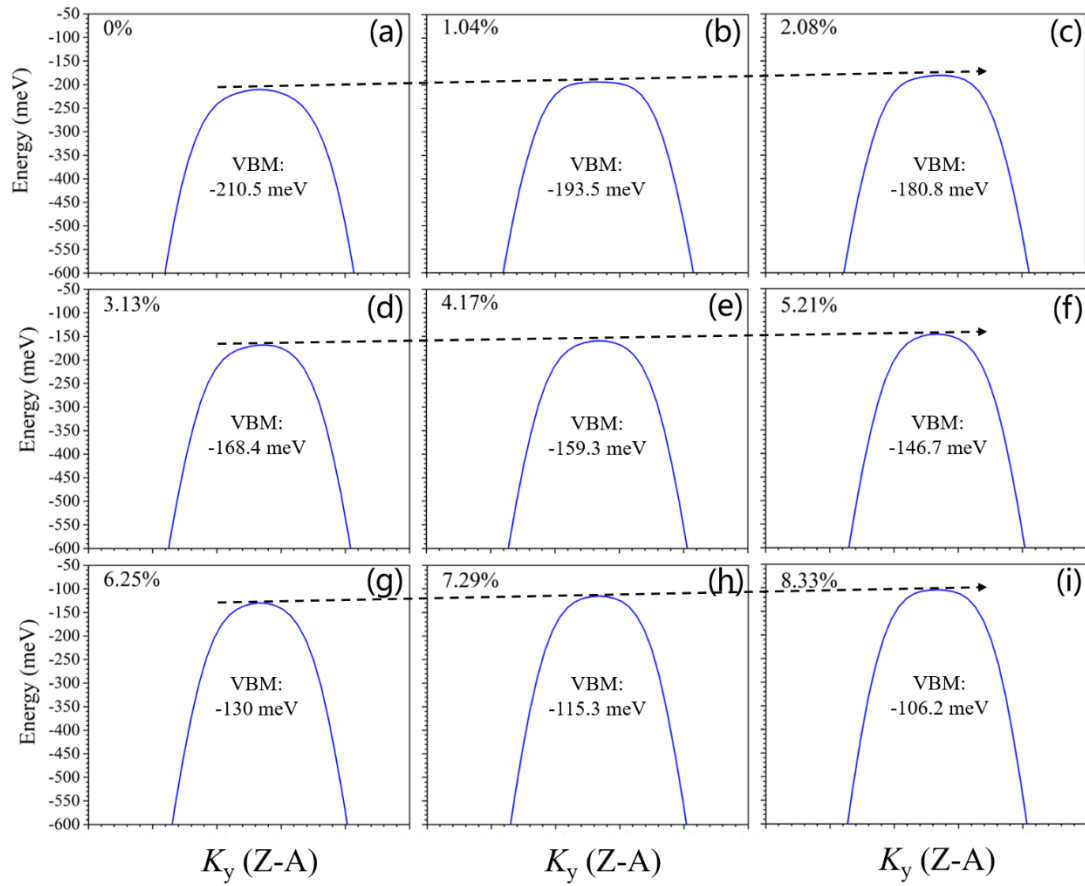


**Figure S4.** The calculated results when tensile strain along zigzag direction.  
(Corresponding to Figure 5c)

#### 4. The effective mass of electrons and band velocity

The tensile strains along armchair and zigzag directions cause an anisotropic shift in VBM, and the VBM shift inevitably leads to changes in the effective mass of electrons and band velocity. As shown in Figure S5, based on experimental and calculated band results, we derived the effective mass and band velocity near VBM as a function of uniaxial tensile strains. The results indicate that when the tensile strains were applied along the armchair direction, with a deeper level shift of the VBM, the effective mass gradually increases and the band velocity gradually decreases. On the other hand, the tensile strains along the zigzag direction reduce the effective mass of electrons and increase the band velocity with the VBM shifts towards shallower levels.

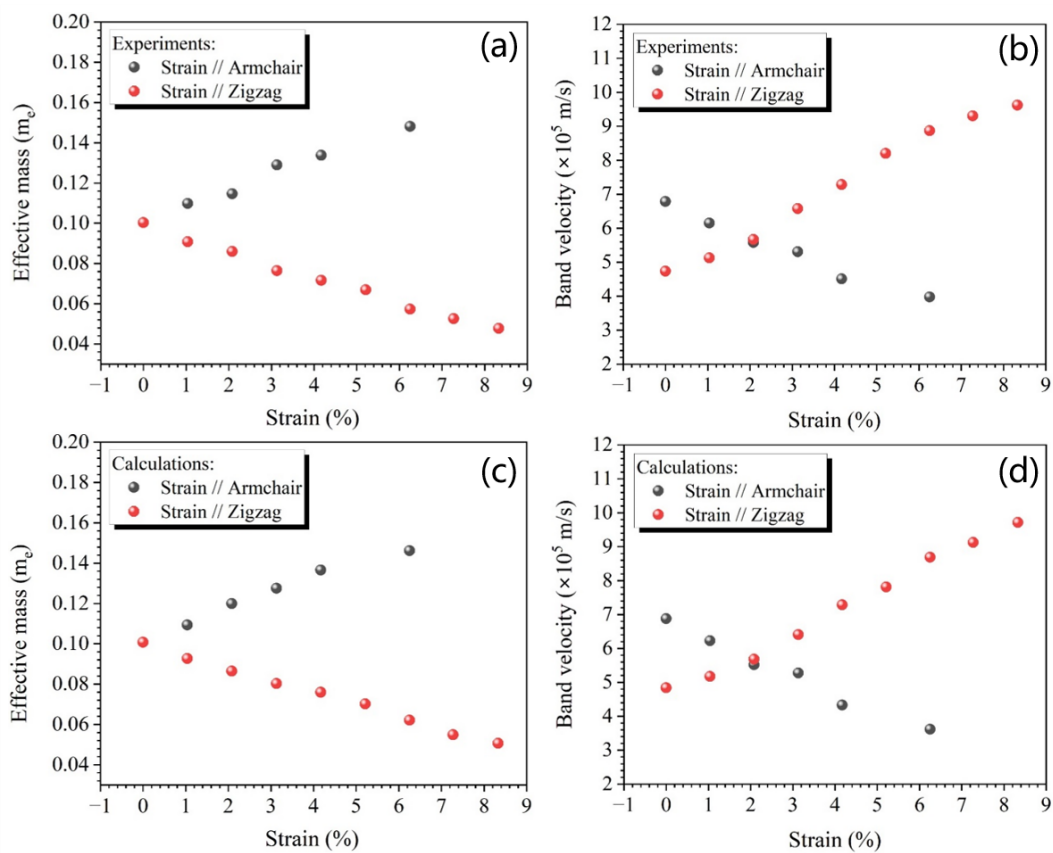


**Figure S5.** The effective mass of electrons and band velocity obtained from the band results of experiments and calculations.

## 5. Strain-ARPES Experiment

At the beginning of measurement, the single-crystalline BP sample (grown from “Muke Nano”) was cleaved in the sample transfer chamber with a base pressure of  $2.8 \times 10^{-8}$  mbar, and then transferred it to the detection chamber of the ARPES system (SPECS PHOIBOS150 analyzer) with a base pressure of  $3.0 \times 10^{-10}$  mbar. The energy and momentum resolutions of the ARPES analyzer were 35 meV and  $0.05 \text{ \AA}^{-1}$ , respectively. The ARPES measurements were performed using the 21.2 eV beamline of a He lamp light source, and the position of the Fermi level was calibrated with a polycrystalline silver.

During the experiments, we used a wobble stick connected to the ARPES system to rotate the screw, which drove the movable anvil to move and achieved *in-situ* adjustment of the sample stretching. The schematic diagram of the experimental process is shown in Figure S6.

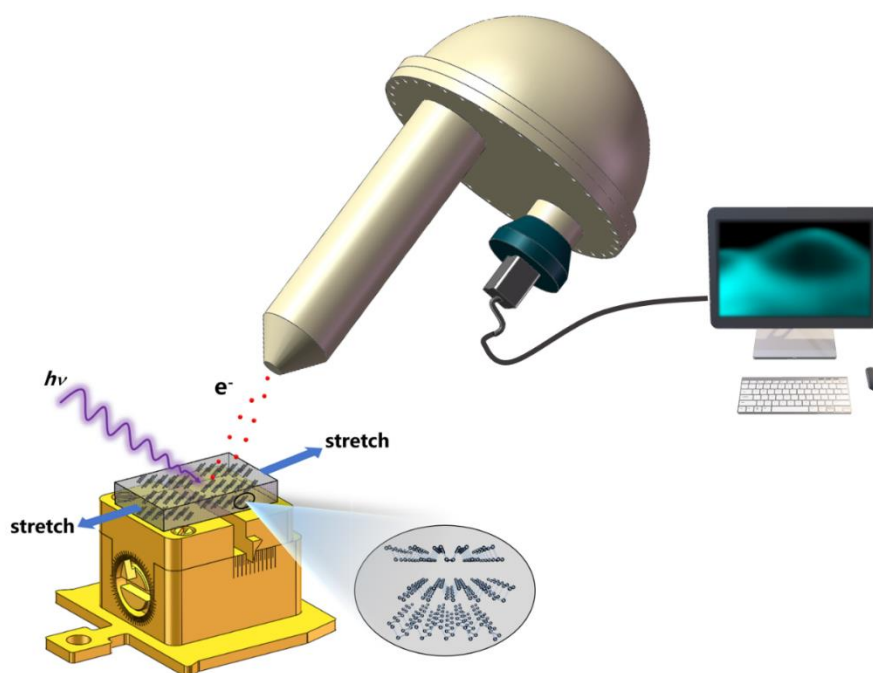


**Figure S6.** Schematic diagram of the experimental process.

## 6. The method of DFT calculation

Density functional theory computations were carried out by Vienna ab initio simulation package (VASP) using the projector augmented wave (PAW) method [7-9]. The exchange correlation potential was represented by the Perdew–Burke–Ernzerhof (PBE) functional within the generalized gradient approximation (GGA) [10]. The cutoff energy for the plane-wave-basis was set to be 450 eV. The k-point sampling grid was set to  $10 \times 3 \times 7$ . We applied 0% - 6.25% uniaxial tensile strain along the armchair direction, and the strain was defined as  $\epsilon_x = (c' - c_0)/c_0$ . And the tensile strain along the zigzag direction ranges from 0% to 8.33%, defined as  $\epsilon_y = (a' - a_0)/a_0$ .  $c_0$  and  $a_0$  are the lattice constants of bulk BP,  $c'$  and  $a'$  are the lattice constants of strained bulk BP. In the process of structural optimization, the crystal axis was tuned along the direction of applied stress, while the other directions were free. The convergence tolerances of energy and force were  $1.0 \times 10^{-5}$  eV/atom and  $2.0 \times 10^{-2}$  eV/Å, respectively. DFT-D3 method was used to describe the van der Waals (vdW) interactions between substrates and adsorbate [11].

## References

- [1] T Takahashi, N Gunasekara, H Ohsawa, H Ishii, T Kinoshita, S Suzuki, and T Sagawa. Angle-resolved photoemission study of black phosphorus: Interlayer energy dispersion[J]. *Phys. Rev. B* 1986, 33(6), 4324.
- [2] A Damascelli. Probing the electronic structure of complex systems by ARPES[J]. *Phys. Scripta* 2006, 2004(T109), 61.
- [3] N Ehlen, B V Senkovskiy, A V Fedorov, A Perucchi, P Di Pietro, A Sanna, G Profeta, L Petaccia, and A Gruneis. Evolution of electronic structure of few-layer phosphorene from angle-resolved photoemission spectroscopy of black phosphorous[J]. *Phys. Rev. B* 2016, 94, 245410.
- [4] T Takahashi, H Tokailin, S Suzuki, and T Sagawa. Highly-angle-resolved ultraviolet photoemission study of a black-phosphorus single crystal[J]. *Phys. Rev. B* 1984, 29(2), 1105.
- [5] S S Baik, K S Kim, Y Yi, and H J Choi. Emergence of two-dimensional massless dirac fermions, chiral pseudospins, and berry's phase in potassium doped few-layer black phosphorus[J]. *Nano Lett.* 2015, 15, 7788.

- [6] H Asahina, K Shindo, and A Morita. Electronic structure of black phosphorus in self-consistent pseudopotential approach[J]. *J. Phys. Soc. JPN.* 1982, 51(4), 1193.
- [7] G. Kresse, D.J. Joubert. From ultrasoft pseudopotentials to the projector augmented wave method[J]. *Phys. Rev.* 1999, 59, 1758.
- [8] G. Kresse, J. Furthmüller. Efficiency of ab-initio total energy calculations for metals and semiconductors using a plane-wave basis set[J]. *Comp. Mater. Sci.* 1996, 6, 15-50.
- [9] G. Kresse, J. Furthmüller. Efficient iterative schemes for ab initio total-energy calculations using a plane-wave basis set[J]. *Phys. Rev.* 1996, 54, 11169.
- [10] J.P. Perdew, K. Burke, M. Ernzerhof. Generalized gradient approximation made simple[J]. *Phys. Rev. Lett.* 1996, 77, 3865.
- [11] K. Lee, É. D. Murray, L. Kong, B. I. Lundqvist, D. C. Langreth. Higher accuracy van der Waals density functional[J]. *Phys. Rev. B* 2010, 82, 081101.